



Article

Interaction of KRSR Peptide with Titanium Dioxide Anatase (100) Surface: A Molecular Dynamics Simulation Study

Tamás Tarjányi ^{1,*} , Ferenc Bogár ² , Janos Minarovits ¹, Márió Gajdács ¹ and Zsolt Tóth ³

¹ Department of Oral Biology and Experimental Dental Research, Faculty of Dentistry, University of Szeged, Tisza Lajos Körút 64-66, H-6720 Szeged, Hungary; minimicrobi@hotmail.com (J.M.); gajdacs.mario@stoma.szote.u-szeged.hu (M.G.)

² MTA-SZTE Biomimetic Systems Research Group, Eötvös Loránd Research Network (ELKH), Dóm tér 8, H-6720 Szeged, Hungary; bogar@sol.cc.u-szeged.hu

³ Department of Experimental Physics, Faculty of Science and Informatics, University of Szeged, Dóm tér 9, H-6720 Szeged, Hungary; ztoth@physx.u-szeged.hu

* Correspondence: tarjanyi.tamas@stoma.szote.u-szeged.hu

Abstract: Due to its tensile strength and excellent biocompatibility, titanium (Ti) is commonly used as an implant material in medicine and dentistry. The success of dental implants depends on the formation of a contact between the oxidized surface of Ti implant and the surrounding bone tissue. The adsorption of proteins and peptides to the implant surface allows the bone-forming osteoblast cells to adhere to such modified surfaces. Recently, it has been observed that tetrapeptide KRSR (Lys-Arg-Ser-Arg) functionalization could promote osteoblast adhesion to implant surfaces. This may facilitate the establishment of an efficient bone-to-implant contact and improve implant stability during the healing process. GROMACS, a molecular dynamics software package was used to perform a 200 ns simulation of adsorption of the KRSR peptide to the TiO₂ (anatase) surface in an aqueous environment. The molecule conformations were mapped with Replica Exchange Molecular Dynamics (REMD) simulations to assess the possible peptide conformations on the anatase surface, and the umbrella sampling method was used to calculate the binding energy of the most common conformation. The simulations have shown that the KRSR peptide migrates and attaches to the surface in a stable position. The dominant amino acid residue interacting with the TiO₂ surface was the N-terminal charged lysine (K) residue. REMD indicated that there is a distinct conformation that is taken by the KRSR peptide. In this conformation the surface interacts only with the lysine residue while the ser (S) and arg (R) residues interact with water molecules farther from the surface. The binding free energy of the most common conformation of KRSR peptide to the anatase (100) surface was $\Delta G = -8.817$ kcal/mol. Our result suggests that the N-terminal lysine residue plays an important role in the adhesion of KRSR to the TiO₂ surface and may influence the osseointegration of dental implants.

Keywords: KRSR; peptide; titanium dioxide; osseointegration; REMD; umbrella sampling; PMF



Citation: Tarjányi, T.; Bogár, F.; Minarovits, J.; Gajdács, M.; Tóth, Z. Interaction of KRSR Peptide with Titanium Dioxide Anatase (100) Surface: A Molecular Dynamics Simulation Study. *Int. J. Mol. Sci.* **2021**, *22*, 13251. <https://doi.org/10.3390/ijms222413251>

Academic Editors: Marco Tatullo, Adriano Piattelli and Barbara Zavan

Received: 15 November 2021

Accepted: 5 December 2021

Published: 9 December 2021

Publisher's Note: MDPI stays neutral with regard to jurisdictional claims in published maps and institutional affiliations.



Copyright: © 2021 by the authors. Licensee MDPI, Basel, Switzerland. This article is an open access article distributed under the terms and conditions of the Creative Commons Attribution (CC BY) license (<https://creativecommons.org/licenses/by/4.0/>).

1. Introduction

Due to its tensile strength, remarkable corrosion resistance, and excellent biocompatibility, titanium (Ti) and its alloys are commonly used as an implant material in medicine and dentistry [1–4]. When exposed to water or air, the surface of Ti is oxidized, and the titanium dioxide (TiO₂) layer formed affects the interaction of Ti implants with various host tissues and cell types [5–7]. In the case of dental implants, the contact between the Ti implant and the surrounding bone tissue is of critical importance, especially in the context of osseointegration [8]. During the initial phase of osseointegration, proteins and peptides adsorb to and modify the implant surface [9]. It was demonstrated that functionalization of TiO₂ surfaces with suitable peptides or proteins could enhance TiO₂–bone interaction and promote the long-term survival of the implants [10,11]. In an in vivo rat tibia model of

implantation, Ti pins coated by type I collagen or the tripeptide RGD (Arg-Gly-Asp; a motif present in several extracellular matrix proteins) attracted higher numbers of macrophages and osteoblasts, compared to unmodified Ti pins [12]. RGD is recognized by integrin proteins located at the membrane of various cell types. Integrin–RGD interactions facilitated cell-adhesion to the extracellular matrix, as well as to RGD-coated Ti surfaces [13–15]. Another peptide, KRSR (Lys-Arg-Ser-Arg) composed of four amino acids, is also suitable for modifying TiO₂ surfaces. KRSR is a heparan-sulfate-binding peptide motif carried by different bone-adhesive proteins [16]. KRSR binds to cell surface proteoglycan molecules and promotes the adhesion of osteoblasts [17–19]. Similarly to their RGD-coated counterparts, KRSR-coated TiO₂ surfaces show enhanced osteogenic differentiation [17–19].

The most common crystalline polymorphs of TiO₂ are rutile, anatase, and brookite. The structure of rutile is tetragonal ($a = b = 0.4584$ nm, $c = 0.2958$ nm), anatase is also tetragonal; compared to rutile, however, the vertical axis of the anatase crystals is longer ($a = b = 0.3782$ nm, $c = 0.9514$ nm), brookite has an orthorhombic structure ($a = 0.5436$ nm, $b = 0.9166$ nm, $c = 0.5135$ nm) [20]. Ti surfaces are covered most commonly by mixtures of anatase and rutile [20]. The Ti implants, used in clinical practice, are treated by acids that favors forming of TiO₂ surface with mainly anatase polymorphic properties [21]. The different surface characteristics of anatase and rutile may affect their interactions with biomolecules [6,11,22,23]. It was suggested that on the anatase (001) surface, the adsorption energy of important peptide motifs carried by bone-adhesive proteins is higher, compared to the rutile (110) surface, which may enhance the osseointegration of Ti implants covered by the anatase polymorph of TiO₂ [22,24,25].

Based on molecular dynamics (MD) simulations, various models were generated describing the interactions of water molecules, amino acids and peptides, including RGD, with TiO₂ surfaces [26–33]. Wu et al. used MD methods to simulate RGD peptide–TiO₂ interaction with two water models (SPC/E and TIP3P) [26]. They used a similar system as our studied model. In their simulation they used rutile while we built up anatase. They found out that the RGD-surface interaction is sensitive to the initial arrangement of the peptide. Song et al. also used MD methods to simulate RGD on rutile surface, they have observed that the RGD adsorbs to the surface by guanidino, amino and carboxyl groups [27]. Wang et al. reviewed studies on MD and Density Functional Theory (DFT) methods for different biomolecule-biomaterial interactions [28]. They compared the hydroxyapatite (HA), TiO₂, and graphene oxide (GO) surfaces and emphasized the importance of water environment in such studies [28]. Sowmiya and Senthilkumar used DFT methods to calculate the binding energy of proline, hydroxyproline and glycine on anatase (001) surface [29]. They found that these amino acids strongly bind to the anatase surface. In a follow-up study, the same authors have also calculated the RGD tripeptide anatase (001) adsorption energies [30]. Luan et al. used MD methods to simulate a nano amorphous TiO₂ sphere particle with a biomolecule [32]. In our study, we utilized the same TiO₂ Lennard-Jones parameters for Ti and O atoms in the TiO₂ surface, as Luan et al. We simulated the anatase-KRSR interactions on molecular level using MD, for which—unlike for the RGD and implant interactions—no previous studies have been performed. In vitro experiments demonstrated, however, that dual-coating of Ti surface with RGD and KRSR peptides enhanced synergistically the differentiation of a human osteoblastic cell line [34]. The aim of our MD simulations was to understand the KRSR behavior on the anatase surface in an aqueous environment and to calculate the binding energy of the predominant adsorption conformation of the peptide.

2. Results and Discussion

2.1. MD Simulation

Firstly, a 200 ns MD simulation was performed. In this simulation the migration and attachment of a KRSR molecule onto the TiO₂ anatase (100) surface in an aqueous environment was modelled. The interaction of water molecules with the TiO₂ surface could already be observed during the first picoseconds of the simulation. The KRSR peptide–TiO₂

surface interactions occurred in the first nanoseconds. As demonstrated on the left side of Figure 1a, the closest atom of the KRSR peptide was initially located at 1.9 nm from the TiO₂ surface. As proposed for the adsorption of peptides to solid surfaces [35,36], the binding of the KRSR peptide to the anatase 100 surface also occurred in three subsequent phases during the simulation. In the first phase of adsorption, which lasted about 1.5 ns (see Figure 1a), the KRSR peptide moved from the bulk water toward the anatase, approaching the water–TiO₂ interface. In Supplementary Material Video S1, this migration phase can be seen in video form. At 1.5 ns, the minimal distance between the peptide and surface was close to 0.2 nm due to non-bonded (van-der Waals and Coulomb) interactions. After 6 ns, the mean minimal distance between the KRSR peptide and the TiO₂ surface fell below 0.2 nm, possibly due to anchoring of the peptide to the surface during the second phase of adsorption (Figure 1a).

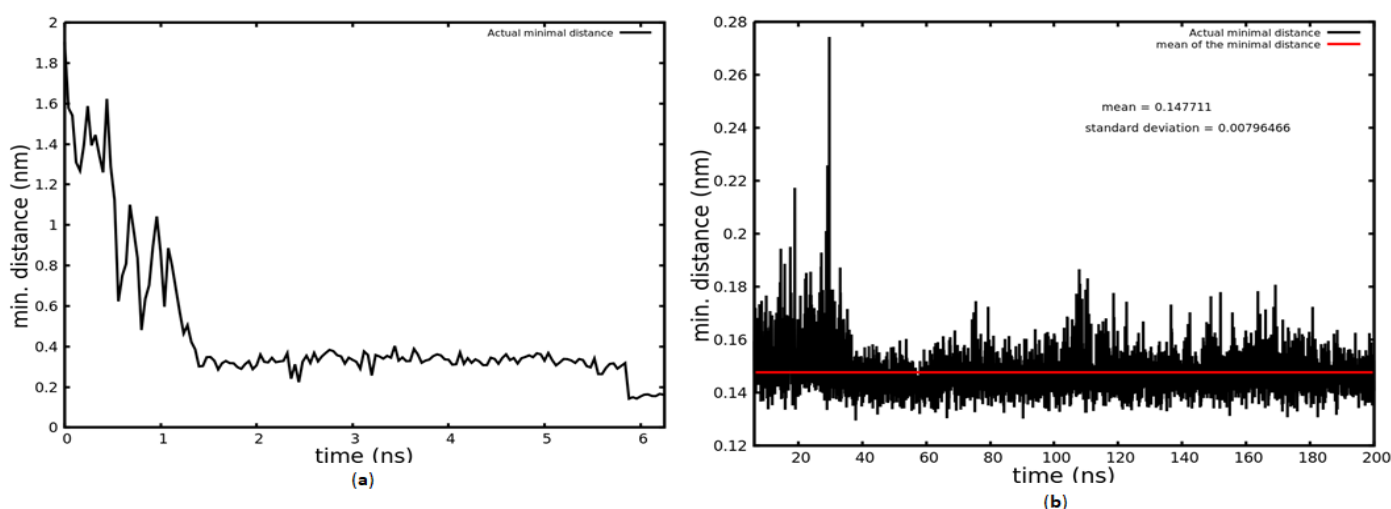


Figure 1. The distance between the TiO₂ surface and the nearest peptide atom over time. In (a), the first 6.25 ns is shown; in (b), the last 193.75 ns is shown.

The KRSR–TiO₂ surface interaction was stable until the end of the simulation. In the last 193 ns, the closest atom of the peptide to the surface oscillated with a 0.02 nm amplitude, at 0.147 nm average distance from the surface. This third phase of adsorption could correspond to lockdown of the peptide to the surface (Figure 1b). Note that, in Figure 1b, a reduced distance scale is used compared to Figure 1a.

The 200 ns simulation showed that the KRSR peptide approached the TiO₂ surface and after 1 ns simulation time it interacted with the surface, mainly with the charged N-terminal lysine residue (see LYS1, Figure 2a). During the second adsorption phase ($t > 6$ ns) the dominant interaction also occurred via the N-terminal lysine residue, as shown on the snapshot in Figure 2b.

We noticed that, in addition to the initial interaction involving the lysine residue, the charged arginine residues (ARG2 and ARG4) also contacted the TiO₂ surface, although less frequently. Figure 2c demonstrates an example of ARG4 and LYS1 contacting the surface simultaneously.

We calculated the Root Mean Square Deviation (RMSD) values of the KRSR peptide over time. The RMSD is the variation of atomic positions compared to the initial structure of the KRSR peptide during the 200 ns simulation. The calculated values indicate that the atomic coordinates of the peptide chain do not change drastically during the simulation. The mean value of the RMSD was 0.116 nm and its standard deviation is 0.016 nm.

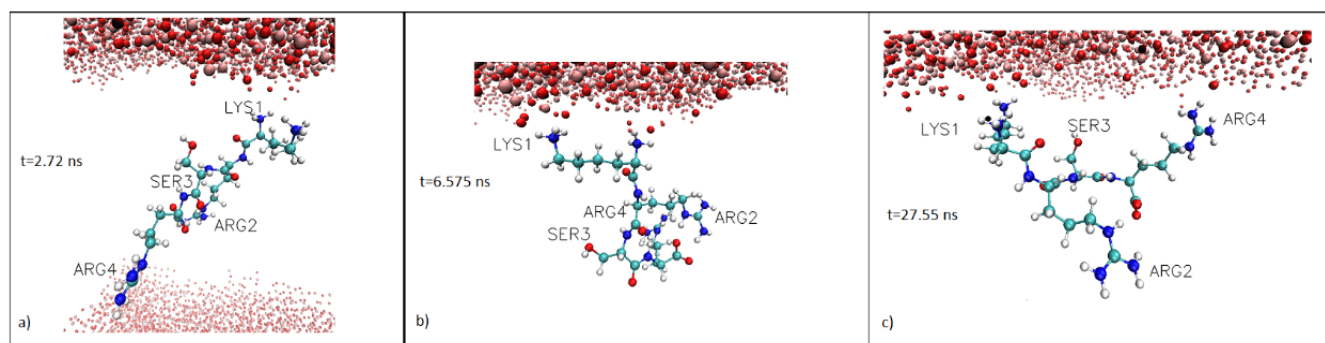


Figure 2. Snapshots from the simulation. (a) time $t = 2.72$ ns (b) time $t = 8$ ns; (c) $t = 27.55$ ns. The snapshots were made without the water molecules. Color code: oxygen, red; nitrogen, dark blue; carbon, cyan; titanium, ochre; hydrogen, gray. Visualization was done with VMD 1.9.3 in CPK representation.

2.2. Determination of Adhered Peptide Conformations by Replica Exchange Molecular Dynamic Simulation (REMD)

REMD simulations were performed on KRSR to investigate the conformational behavior of the peptide at different temperatures. A total of 96 replicas were used in the temperature range of 310–454 K, and the final analysis was performed for the replica at 310 K. The linkage clustering method was used, with a 0.1 nm RMSD cutoff to determine different molecular conformations of the KRSR on the surface. Conformational analysis of the KRSR provided insight into the unstable and disordered structures of the KRSR. Figure 3 shows the distribution of the occurrence of peptide molecule conformations for the first 58 clusters, which were the most populated. The different molecular cluster conformations were determined by the RMSD.

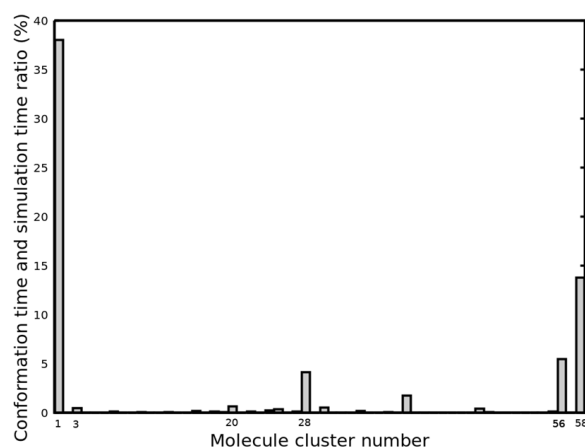


Figure 3. Cluster populations of the different KRSR peptide conformations, based on the lowest temperature simulation.

The four most prevalent KRSR peptide conformations identified by the clustering process corresponded to cluster number 1 (cluster size: 4751), 28 (cluster size: 516), 56 (cluster size: 685), and 58 (cluster size: 1724), respectively; their molecular geometries are displayed in Figure 4. In total, 468 clusters were found and 4539 transitions were recorded. All four conformations contacted the surface through the N-terminal lysine residue (Lys1), however, conformation 56 and 28 also adhered with the second residue (Arg2).

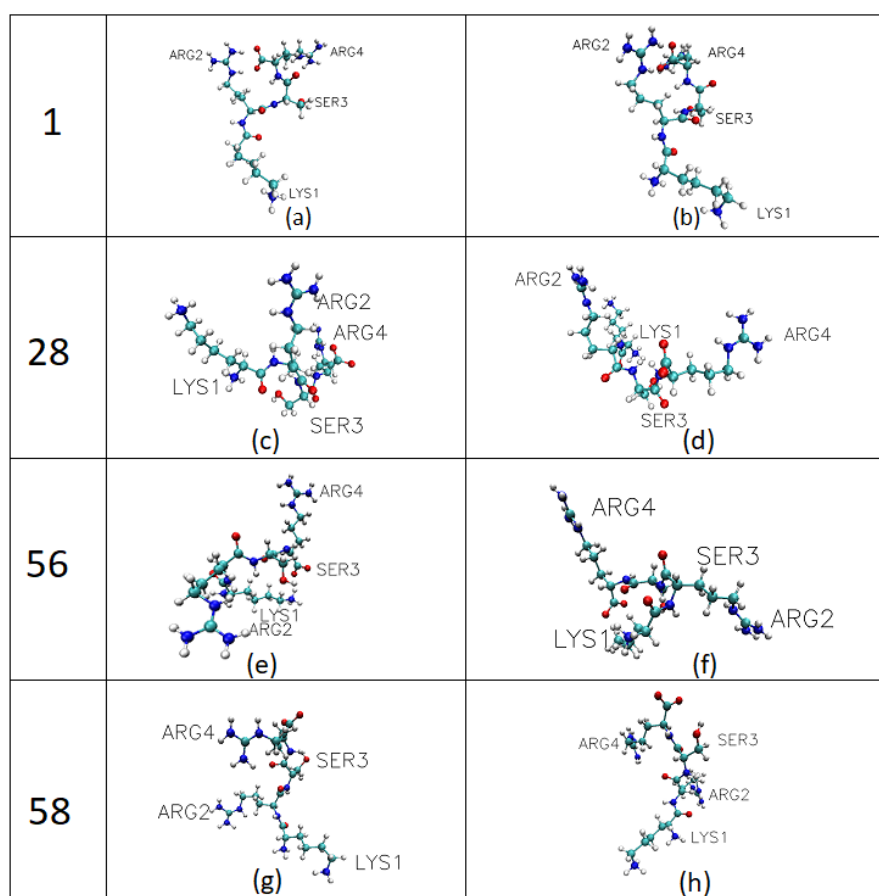


Figure 4. Molecular conformations of the KRSR peptide viewed from two different angles. The four most prevalent conformations identified by REMD simulations are shown. (a,b) are views from different directions of KRSR conformation cluster number 1, (c,d) are views of cluster number 28, (e,f) shows the conformation of cluster number 56 and (g,h) belongs to conformation of cluster number 58. Visualization was done with VMD 1.9.3 in CPK representation.

2.3. Binding Free Energy Calculation by Potential of Mean Force (PMF) Calculation

Based on the results obtained from REMD simulations, we used the most dominant conformation to pull it from the surface. The magnitude of the force required for pulling the KRSR molecule (cluster No.: 1) is shown in Figure 5. This is done by attaching an imaginary spring to the center of mass (COM) of the molecule, which is pulled along the z-axis perpendicular to the TiO₂ surface. The spring constant was defined as 1000 kJ·nm⁻¹·mol⁻¹, which is the usual value for pull procedures. The rate of pulling was set to a constant value of 5 nm/ns, which is comparable to the velocity of molecular motion in fluids. During the pull-simulation, interactions occur (i) between the anatase surface and the peptide, and (ii) between the surrounding water molecules and the peptide. The pulling procedure lasted up to 1 ns. During pulling, up to 0.2 ns, the center of the molecule moves away from the surface, which can be seen in the Supplementary Material Video S2. The molecule elongates and at 0.2 ns the peptide-TiO₂ surface interaction ceases, and the molecule then has close contacts only with the surrounding water molecules. In Figure 5a, at 0.2 ns this is accompanied by a sudden decrease in force. In Figure 5b, the Z position of the center of mass of KRSR molecule is shown as a function of time. The position value starts from 3.8 nm since the surface Z position ends roughly at this value. During the elongation period the position value gradually increases and at 0.2 ns a sudden sub nm increase can be observed, which is in correlation with the force–time curve. This sudden increase refers to that moment, when the elongated peptide is torn from the surface and contracts. After

0.2 ns, the position of the peptide generally corresponds to the 5 nm/ns pulling velocity, and the interactions with the water surrounding can be seen as the noise on the curve.

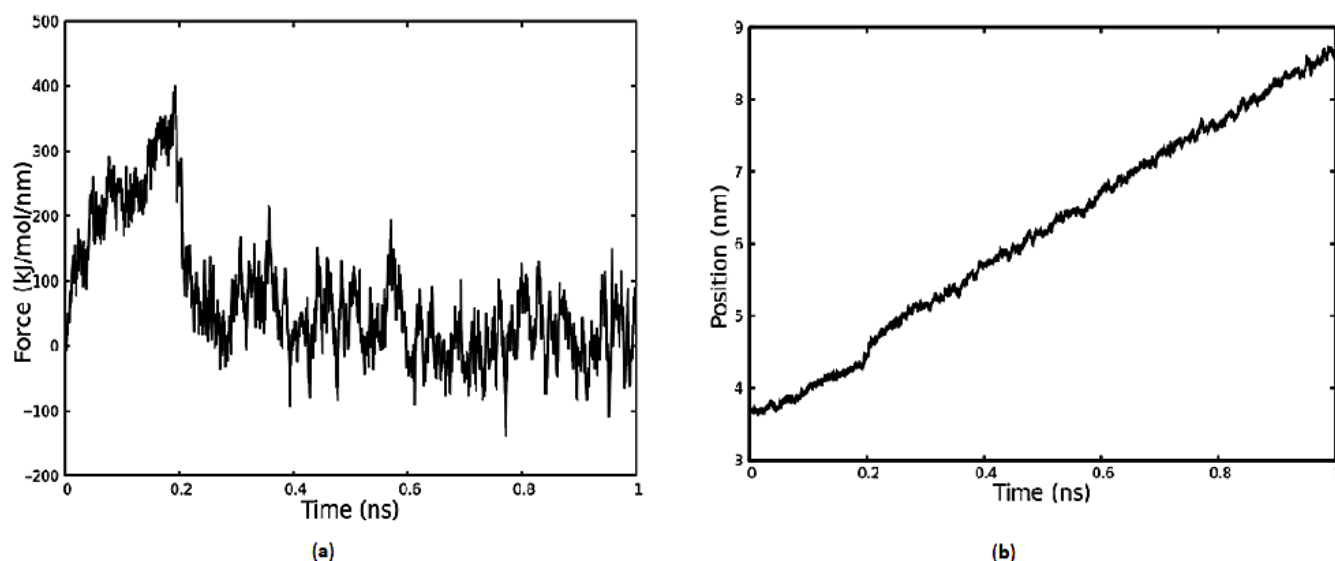


Figure 5. In (a), the force that is necessary to pull the KRSR peptide's center of mass is represented as a function of time. In (b), the z coordinate of the peptide's center of mass is depicted as a function of time. The surface of the TiO_2 slab is between 0 and 3.5 nm.

During the pull simulation we recorded the atomic positions of the system for the umbrella sampling procedure. The center of mass of the peptide was fixed in 24 different positions with a harmonic potential at different points along the pull axis. These points were taken further away from one after the other. We ran independent molecular dynamics simulations with these fixed KRSR systems where the position of COM of the peptide could be displaced due to the interaction with water molecules. The distribution of the displacements gives an umbrella-type curve at each position. The results of the umbrella sampling are shown in Figure 6 in a histogram form. This histogram displays the distribution of the distances taken by the COM of the KRSR peptide from the TiO_2 surface at the 24 fixed positions described above, during the 10 ns sampling.

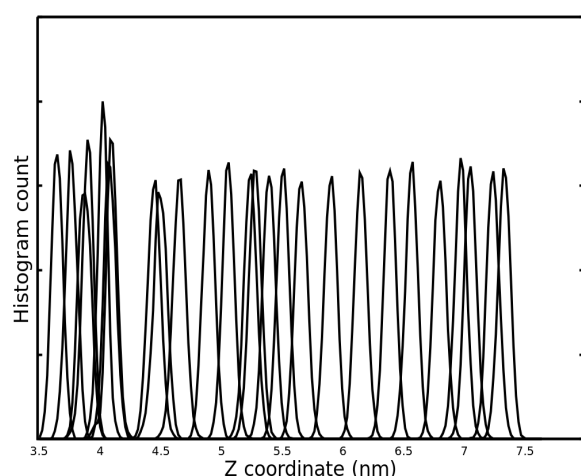


Figure 6. Distribution of the distances taken by the KRSR peptide's center of mass from the TiO_2 surface at different fixed points during the 10 ns sampling.

Finally, the Weighted Histogram Analysis Method (WHAM) algorithm [37] was used to analyze the results of the umbrella sampling method. As a result, we obtained the potential of mean force (PMF) curve shown in Figure 7. The highest and lowest values correspond to the ΔG value of the bonding/release process. The binding free energy ΔG was established, based on the PMF profile shown. Thus, ΔG , the binding free energy of the KRSR peptide to the anatase (100) surface obtained, was -8.817 kcal/mol (-36.89 kJ/mol).

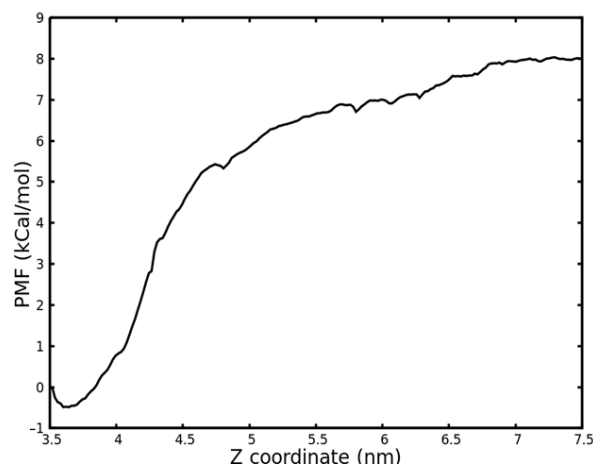


Figure 7. Potential of Mean Force (PMF) energy values of the simulated KRSR peptide–TiO₂ surface interaction as a function of the Z coordinate.

2.4. Discussion

Biomolecules bound to the surface of Ti implants covered by TiO₂ may facilitate successful integration of both surgical and dental implants into the surrounding bone tissue [11,38,39]. It was demonstrated that distinct proteins and peptides attached to TiO₂ surfaces enhance migration, proliferation, and differentiation of osteoblasts, which may play a prominent role in bone formation [12,17,23,34,40,41]. In addition to *in vivo* and *in vitro* studies, molecular dynamics simulations are also indispensable for the understanding of the complexities of peptide–water–solid surface interactions involved in osseointegration of implants [22,35,42–44].

We have performed MD simulations to study the adsorption of the KRSR peptide to the anatase (100) surface in aqueous environment. Three phases of KRSR binding were observed. In the initial phase (Phase 1), lasting for 1.5 ns, the peptide moved from the bulk water toward the anatase surface. This corresponds to a migration speed of ~ 1.14 m/s. In Phase 2, from 1.5 ns to 6 ns, the peptide was anchored at about 0.2 nm from the surface. Firstly the lysine (K) part of the peptide interacted with the surface. This interaction led to anchoring of the peptide to the surface, which showed stable binding in the second and third phase of adsorption. In Phase 3 (lockdown; from 6 ns to 200 ns), the KRSR peptide stayed stably in the vicinity of the anatase 100 surface: its closest atom was located at an average of 0.147 nm from the surface till the end of the simulation. Our prolonged, 200 ns simulation revealed that the initial KRSR–TiO₂ (anatase 100) surface interaction was mediated by the N-terminal lysine (K) residue of the peptide. It was also observed that, in certain time periods, the two charged arginine (R) residues, Arg2, which is next to the Lys1, and the carboxy terminal Arg4 residue also interacted with the surface. The fluctuations of the peptide geometry, having an average amplitude of 0.02 nm, can be attributed to the dynamic interactions between the peptide, surface, and water molecules. These observations are compatible with the results of Sultan et al., who applied molecular dynamics simulations and metadynamics to calculate the binding affinities of distinct amino acid analogues to the charged, aqueous rutile (110) surface [45]. They found that at neutral pH the ranking order of the strongest binder side chain analogues was “arginine”, “lysine”, “aspartic acid”, and “serine” [45].

We assessed the most probable molecular conformations of the KRSR peptide using REMD (Replica Exchange Molecular Dynamics) simulations and selected the most likely conformation to calculate the binding energy characteristic for the KRSR-anatase (100) interaction. Figure 3 shows that cluster 1 appears in almost 40% of simulation times, as shown in Figure 8 as well.

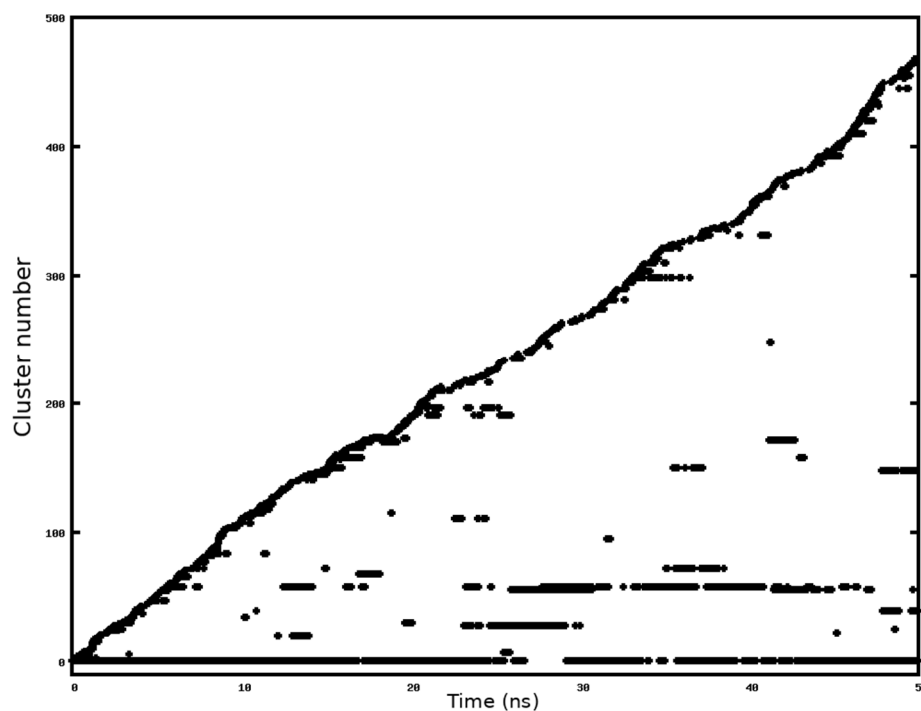


Figure 8. Changes in cluster populations of the different KRSR peptide conformations during the REMD simulation.

Figure 8 demonstrates how the most prevalent molecular configurations (clusters) change over the REMD simulation. Although cluster 1 was present from the beginning of the simulation, new molecular conformations also occurred due to the interactions with the TiO_2 surface and water molecules. Furthermore, during the higher temperature simulations the molecule coordinates can replica change with a certain probability. It is also visible that the KRSR peptide during this simulation reverts to more favorable conformations (to the previously discussed four dominant conformations shown in Figure 4).

Out of the four most common conformations, No. 1 and 58, (No. 58 is the second most common manifestation) are similar in that only the N-terminal lysine residue (Lys1) adheres to the surface. However, at conformations 56 and 28, arginine (Arg2) also adheres in addition to Lys1, forming a bridge; whereas Ser3 and Arg4 residues interact with the surrounding water molecules farther away from the surface.

Pulling of the KRSR molecule in aqueous environment and the umbrella sampling procedure were used to calculate the binding free energy of the KRSR to the anatase 100 surface. Figures 5b and 6 shows the detachment of the molecule from the surface when applying an elastic force that is maintained by a harmonic potential. In Figure 5b, a sudden change was observed at 0.2 ns time point indicating the detachment of the molecule from the TiO_2 surface. As demonstrated in Figure 6, the distributions of the distances (normal distributions) at different time points are evenly dispersed along the Z coordinates. However, when the center of mass of the KRSR molecule is between 4 and 4.5 nm, a rarefaction can be observed. Both curves indicate the disintegration of the peptide from the surface. Our main result is the determination of the ΔG , the binding free energy of the KRSR peptide to the anatase (100) surface for which the -8.817 kcal/mol (-36.89 kJ/mol)

value was obtained. This value is in the expected range compared to the results of other TiO₂-molecule binding energy studies.

Luan et al. analyzed the interaction of the SH3 domain (SRC-homology 3 domain, derived from an adaptor protein) with a TiO₂ amorphous nanoparticle [32]. In their study they verified the very same Lennard-Jones potential parameters of Ti and O as used in this work. Brandt and Lyubartsev et al. applied the umbrella sampling method to calculate the free energy profiles and the adsorption free energies of 19 amino acids on the rutile (100) TiO₂ surface [46]. It is worth noting, however, that the polar side chain analogues of the amino acids serine (Ser, S) and threonine (Thr, T) were able to penetrate the tightly-bound water layer on the TiO₂ (rutile, 100) surface and bind to TiO₂ [46]. Arcangeli et al. used DFT and MD methods to see the structure and stability of single amino acids; they also used MD methods to investigate the adsorption of the 13-residue sequence AMRKLPDAPGMHC by pulling it away from the surface [47]. They used a method similar to the one we used to pull the KRSR peptide from the surface in our study. Previously Lemkul et al. used the umbrella sampling and pulling method to calculate binding free energies protofibrils [48]. In their study they pulled away peptide parts, this is also very similar how we performed our pulling method and umbrella sampling.

Muir et al. used DFT methods to investigate the RGD binding energy on the TiO₂ rutile (110) surface [49]. Their data indicated that the peptide adsorbs via the carboxyl group of the aspartic acid residue to the surface. In their study it was found that the RGD O atom made a sigma bond with the surface Ti atom. Sowmiya et al. also used DFT methods to investigate the adsorption of RGD but on an anatase TiO₂ (001) surface [30]. They found that the adsorption energy for RGD is higher on anatase than on the rutile surface and concluded that the anatase surface is more favorable for implant functionalization. The maximum adsorption energy in their study for RGD on the anatase surface was -1.62 eV (-6.2 kcal/mol = -25.94 kJ/mol), which is consistent with our result, KRSR anatase adsorption energy (-8.817 kcal/mol). Thus, although the adsorption energies were determined by different methods, the results were, in a way, comparable for these charged oligopeptides.

As far as we know, this is the first attempt to determine the binding energy of the KRSR peptide to TiO₂ (anatase) surface. Regarding peptide-TiO₂ surface interactions, most of the molecular dynamics studies and DFT calculations focused on the binding of RGD peptide to TiO₂ polymorphs, rutile and anatase. The RGD sequence is present in several extracellular matrix (ECM) proteins and mediates ECM-cellular receptor interactions [13–15]. Zhang et al. calculated that the binding energy of RGD is higher for the anatase (101) surface than to the rutile (110) surface [22]. They argued that the presence of Ti atoms on the surface of the anatase positively affects the surface adsorption of the RGD peptide, while on the oxygen-terminated rutile surface the interaction with oxygen atoms is weaker [22]. In addition, comparison of the RGD binding energy in vacuum and water revealed that the presence of water molecules may interfere with the adsorption of the peptide to TiO₂ surfaces [22]. We have also observed that water affects the binding of KRSR, and the binding of the ϵ -amino group of the N-terminal lysine occurs mostly between the oxygen atom of the TiO₂ surface or the surface-bound water. The results of Schneider et al. are consistent with this observation, they found that RGD binding to the TiO₂ surface is mediated predominantly by the arginine (R) residue located to the N-terminal end of the peptide [50]. They suggested, however, that the C-terminal asparagine (D) also plays a role in the surface association as well, in accordance with the proposal by Guo et al. [50,51]. It has to be noted that the integrin-binding RGD motif interacted with a subset of integrin family receptors expressed on the surface of a variety of cell types [52]. In contrast, the heparin-binding tetrapeptide KRSR preferentially stimulated the adhesion of osteoblasts to KRSR-coated surfaces [17–19,34]. We observed that during molecular simulation the KRSR peptide attached to the TiO₂ (anatase) surface predominantly via its N-terminal lysine (K) residue, whereas the serine (S) and arginine (R) residues interacted with water molecules. This observation suggests that the KRSR motifs carried by certain extracellular

matrix proteins may also interact with titanium surfaces via the side-chain amino group of lysine residues and may also facilitate the design of biomimetic surfaces enhancing osseointegration of dental or surgical implants.

3. Materials and Methods

Molecular dynamics (MD) simulations were performed with GROMACS (2018.3 version) [53–60]. The CHARMM36 force field [61,62] was applied to set up the parameter files for the KRSR and its surrounding environment. This force field is suitable for generating polypeptide backbone conformational ensembles for intrinsically disordered peptides and proteins. The simulation space was a 4.5 nm × 8.3 nm × 11 nm box. This space was convenient to define the TiO₂ crystal lattice. The space above the Ti surface was filled with the peptide, water, and a few ions (Na⁺ and Cl[−]) to maintain the neutrality. The TiO₂ crystal structure (100) started from z = 0 nm until z = 4 nm. The simulation box was set to have a periodic boundary condition in order to simulate a large space. This was necessary to make the peptide and the molecules in the solution able to migrate over the boundary. For the setting up of the TiO₂ crystal, the unit cell of anatase was used. The structure of unit cell was obtained from the American Mineralogist Crystal Structure Database recorded by Howard [63]. The KRSR peptide initial geometry was created with the program Gabedit 2.5.0 [64]. After the creation process, an energy minimization was performed on the peptide with the Quasi Newton gradient method (Amber potential). At the beginning of the molecular dynamics simulation, the position of the KRSR peptide was set to the middle of the x-y plain and ~1.9 nm distance from the anatase surface. The simulation system contained 7625 water molecules and the TIP3P explicit water model [65] was applied on them. The initial geometry of the system is shown in Figure 9a.

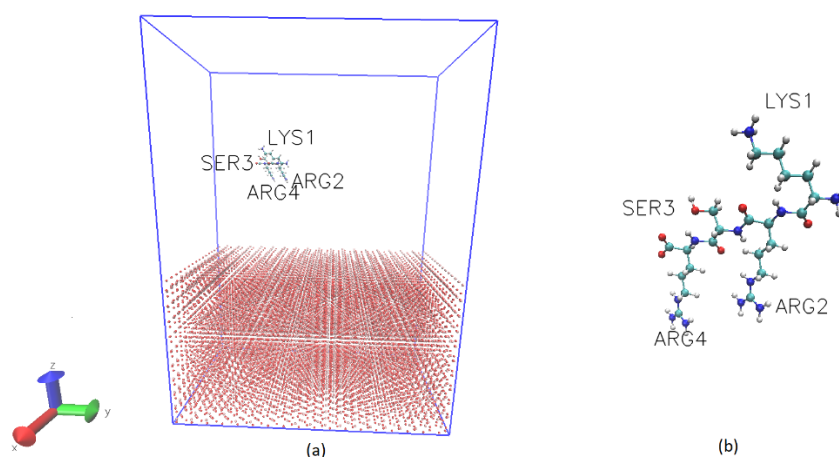


Figure 9. Snapshots of the initial geometry of the simulated system: **(a)** The left snapshot shows the TiO₂ crystal structure and the KRSR peptide, without the water molecules, the blue box represents the periodic boundary; **(b)** The right snapshot shows the initial KRSR peptide geometry. Color code: oxygen, red; nitrogen, dark blue; carbon, cyan; titanium, ochre; hydrogen, gray. Visualization was done with VMD 1.9.3 in CPK representation.

During the simulation, a cut off distance of 1 nm was applied for the electrostatic and van der Waals forces. The van der Waals potential for TiO₂ was described with the usual Lennard-Jones potential parameters as described by Luan et al. [32] (Equation (1)):

$$U(r_{ij}) = \varepsilon_{ij} \left[\left(\frac{\sigma_{ij}}{r_{ij}} \right)^{12} - 2 \left(\frac{\sigma_{ij}}{r_{ij}} \right)^6 \right] + \frac{q_i q_j}{r_{ij}} \quad (1)$$

where the first part in Equation (1) is the Lennard-Jones potential and the second part is the Coulomb potential, r_{ij} is the distance between two atoms, ϵ_{ij} is the well depth of the potential energy, σ_{ij} is the size of the particles, q_i is partial charges.

The following parameters were used to set the Lennard-Jones potential parameters for the Ti and O atoms in the anatase crystal: $\epsilon_{\text{Ti-Ti}} = 0.58$ kcal/mol, $\epsilon_{\text{Ti-O}} = 0.424$ kcal/mol, $\epsilon_{\text{O-O}} = 0.58$ kcal/mol, $\sigma_{\text{Ti-Ti}} = 0.220$ nm, $\sigma_{\text{Ti-O}} = 0.272$ nm, $\sigma_{\text{O-O}} = 0.324$ nm and the partial charges $q_{\text{Ti}} = 2.196$ e, $q_{\text{O}} = -1.098$ e. The potential parameters for the atoms in the solution were already defined by the CHARMM36 force field. The simulation protocol started with a usual energy minimization in 2000 steps to relax the initial structure. After this, the temperature of the system was increased from 0 K up to 310 K and the equilibration was done in two phases. During the first phase an isothermal-isochoric (Number of particles, Volume, and Temperature are all constant: NVT) process was done over 500 ps. The system was heated up in two different groups: (i) atoms of the anatase crystal and (ii) the peptide–water components. These two groups of atoms were treated like this during all simulation processes. The temperature was controlled via Langevin dynamics [66]. The equilibrium searching process continued with the isothermal-isobaric equilibration (Number of particles, Pressure and Temperature are all constant: NPT) during another 100 ps. A 200 ns MD simulation started after this point at 310 K and 1 bar pressure. The time step during the NVT and NPT equilibration processes were 1 fs, while it was 2 fs during the MD. During the simulations there was no extra restrictions for the TiO₂ atoms. The atoms stayed near at their crystal lattice points and vibrated there with the given kinetic energy.

For REMD (Replica Exchange Molecular Dynamics) simulations, 96 replicas were used to find the incidence of different conformations of the KRSR molecule. The temperature difference was 1.5 K, starting at 310 K on the lowest temperature thread. The initial system for the REMD was taken from the result of the 200 ns MD simulation. The replicas were equilibrated (NPT) over 1.25 ns. After the equilibration we performed a 50 ns parallel simulation on the replicas. During the equilibration and REMD simulations the time step was 2 fs. The replica exchange could take place at each 500th step, i.e., at 1 ps intervals. The replica exchange only replaced the atomic coordinates of the peptide by adjacent temperature simulations. The probability of replacements throughout the simulation was around 0.3. By examining the lowest temperature thread, the prevalence of distinct peptide conformations was assessed with a 0.1 nm cut-off single linkage clustering.

The Potential Mean Force (PMF) simulations were performed using conformation 1, the most abundant conformation observed during REMD (Figure 4a). During the PMF calculations the simulation box was extended in the z axis to 18 nm. The size of the new, extended simulation box was 4.5 nm × 8.3 nm × 18 nm. As a first step, the center of mass of the KRSR peptide was pulled from the TiO₂ surface to a distance of 5 nm, over 1 ns. The z coordinate represents the COM coordinate of KRSR at the z axis, which is perpendicular to the plane of the anatase–water interface. After this process at 24 selected points the COM of KRSR position was fixed with a harmonic force. At these points, umbrella sampling was performed with a potential energy well depth of 1000 kJ·mol⁻¹·nm⁻², as described in the literature [48,67]. The equilibrium state search lasted 1.2 ns, after this a 10 ns MD simulation was performed with a 2 fs time step. To create the PMF profile the WHAM (weighted histogram analysis method) module of GROMACS was applied on the 24 selected umbrella samples [34]. Based on our umbrella sampling simulations, the binding energy of the KRSR peptide to the surface of the anatase was determined.

Supplementary Materials: The following are available online at <https://www.mdpi.com/article/10.3390/ijms222413251/s1>.

Author Contributions: Conceptualization, J.M., Z.T.; methodology T.T., F.B., Z.T.; calculations, T.T.; writing—original draft preparation, T.T.; writing—review and editing, T.T., Z.T., J.M., M.G., F.B.; visualization, T.T.; supervision, Z.T., J.M.; funding acquisition, M.G., J.M. All authors have read and agreed to the published version of the manuscript.

Funding: This work was supported by the grant GINOP-2.3.2-15-2016-00011 to a consortium led by the University of Szeged, Szeged, Hungary (participants: the University of Debrecen, Debrecen, Hungary and the Biological Research Centre, Hungarian Academy of Sciences, Szeged, Hungary), project leader János Minárovits. The grant was funded by the European Regional Development Fund of the European Union and managed in the framework of Economic Development and Innovation Operational Programme by the Ministry of National Economy, National Research, Development and Innovation Office, Budapest, Hungary. M.G. was supported by the János Bolyai Research Scholarship (BO/00144/20/5) of the Hungarian Academy of Sciences. The research was supported by the ÚNKP-21-5-540-SZTE New National Excellence Program of the Ministry for Innovation and Technology from the source of the National Research, Development and Innovation Fund. M.G. would also like to acknowledge the support of ESCMID's "30 under 30" Award.

Institutional Review Board Statement: Not applicable.

Informed Consent Statement: Not applicable.

Data Availability Statement: External data sources used in this study are cited in article. All data generated during the study are presented in this paper and its supplementary materials.

Acknowledgments: We acknowledge KIFÜ for awarding us access to the HPC resources based in Hungary.

Conflicts of Interest: The authors declare no conflict of interest, monetary or otherwise. The authors alone are responsible for the content and writing of this article.

References

1. Yvoni, K.; Margarita, S.; Maria-Eleni, D.; Bennani, V.; Bakopoulou, A.; Tsouknidas, A.; Michailidis, M.; Michalakis, K. New Ti-Alloys and Surface Modifications to Improve the Mechanical Properties and the Biological Response to Orthopedic and Dental Implants: A Review. *BioMed Res. Int.* **2016**, *2016*, 2908570.
2. Collet, T.; Atanasiu, J.P.; de Cussac, J.B.; Oufroukhi, K.; Bothorel, H.; Saffarini, M.; Badatcheff, F. Midterm outcomes of titanium modular femoral necks in total hip arthroplasty. *Ann. Transl. Med.* **2017**, *5*, 395. [[CrossRef](#)]
3. Kruyt, I.J.; Nelissen, R.C.; Mylanus, E.A.M.; Hol, M.K.S. Three-year Outcomes of a Randomized Controlled Trial Comparing a 4.5-mm-Wide to a 3.75-mm-Wide Titanium Implant for Bone Conduction Hearing. *Otol. Neurotol.* **2018**, *39*, 609–615. [[CrossRef](#)] [[PubMed](#)]
4. Jung, R.E.; Pjetursson, B.E.; Glauser, R.; Zembic, A.; Zwahlen, M.; Lang, N.P. A systematic review of the 5-year survival and complication rates of implant-supported single crowns. *Clin. Oral Implant. Res.* **2008**, *19*, 119–130. [[CrossRef](#)]
5. Li, L.H.; Kong, Y.M.; Kim, H.W.; Kim, Y.W.; Kim, H.E.; Heo, S.J.; Koak, J.Y. Improved biological performance of Ti implants due to surface modification by micro-arc oxidation. *Biomaterials* **2004**, *25*, 2867–2875. [[CrossRef](#)] [[PubMed](#)]
6. Li, A.; Wang, Z.; Yin, H.; Wang, S.; Yan, P.; Huang, B.; Wang, X.; Li, R.; Zong, X.; Han, H.; et al. Understanding the anatase–rutile phase junction in charge separation and transfer in a TiO₂ electrode for photoelectrochemical water splitting. *Chem. Sci.* **2016**, *7*, 6076–6082. [[CrossRef](#)]
7. Ong, J.; Lucas, L.C.; Raikar, G.N.; Connatser, R.; Gregory, J.C. Spectroscopic characterization of passivated titanium in a physiologic solution. *J. Mater. Sci. Mater. Electron.* **1995**, *6*, 113–119. [[CrossRef](#)]
8. Lavenus, S.; Louarn, G.; Layrolle, P. Nanotechnology and Dental Implants. *Int. J. Biomater.* **2010**, *2010*, 915327. [[CrossRef](#)]
9. Miller, R.; Guo, Z.; Vogler, E.A.; Siedlecki, C.A. Plasma coagulation response to surfaces with nanoscale chemical heterogeneity. *Biomaterials* **2006**, *27*, 208–215. [[CrossRef](#)]
10. Ferris, D.M.; Moodie, G.D.; Dimond, P.M.; Gioranni, C.W.; Ehrlich, M.G.; Valentini, R.F. RGD-coated titanium implants stimulate increased bone formation in vivo. *Biomaterials* **1999**, *20*, 2323–2331. [[CrossRef](#)]
11. Chen, S.; Guo, Y.; Liu, R.; Wu, S.; Fang, J.; Huang, B.; Li, Z.; Chen, Z.; Chen, Z. Tuning surface properties of bone biomaterials to manipulate osteoblastic cell adhesion and the signaling pathways for the enhancement of early osseointegration. *Colloids Surf. B Biointerfaces* **2018**, *1*, 58–69. [[CrossRef](#)] [[PubMed](#)]
12. Rammelt, S.; Illert, T.; Bierbaum, S.; Scharnweber, D.; Zwipp, H.; Schneiders, W. Coating of titanium implants with collagen, RGD peptide and chondroitin sulfate. *Biomaterials* **2006**, *27*, 5561–5571. [[CrossRef](#)] [[PubMed](#)]
13. Pierschbacher, M.D.; Ruoslahti, E. Cell attachment activity of fibronectin can be duplicated by small synthetic fragments of the molecule. *Nat. Cell Biol.* **1984**, *309*, 30–33. [[CrossRef](#)] [[PubMed](#)]
14. Ruoslahti, E. Control of cell motility and tumour invasion by extracellular matrix interactions. *Br. J. Cancer* **1992**, *66*, 239–242. [[CrossRef](#)] [[PubMed](#)]
15. Hersel, U.; Dahmen, C.; Kessler, H. RGD modified polymers: Biomaterials for stimulated cell adhesion and beyond. *Biomaterials* **2003**, *24*, 4385–4415. [[CrossRef](#)]
16. Cardin, A.D.; Weintraub, H.J. Molecular modeling of protein-glycosaminoglycan interactions. *Arteriosclerosis* **1989**, *9*, 21–32. [[CrossRef](#)]

17. Dee, K.C.; Andersen, T.T.; Bizios, R. Design and function of novel osteoblast-adhesive peptides for chemical modification of biomaterials. *J. Biomed. Mater. Res.* **1998**, *5*, 371–377. [[CrossRef](#)]
18. Hasenbein, M.E.; Andersen, T.T.; Bizios, R. Micropatterned surfaces modified with select peptides promote exclusive interactions with osteoblasts. *Biomaterials* **2002**, *23*, 3937–3942. [[CrossRef](#)]
19. Balasundaram, G.; Webster, T.J. Increased osteoblast adhesion on nanograined Ti modified with KRSR. *J. Biomed. Mater. Res. A* **2007**, *1*, 602–611. [[CrossRef](#)]
20. Diebold, U. The surface science of titanium dioxide. *Surf. Sci. Rep.* **2003**, *48*, 53–229. [[CrossRef](#)]
21. Sul, Y.T.; Johansson, C.B.; Petronis, S.; Krozer, A.; Jeong, Y.; Wennerberg, A.; Albrektsson, T. Characteristics of the surface oxides on turned and electrochemically oxidized pure titanium implants up to dielectric breakdown: The oxide thickness, micropore configurations, surface roughness, crystal structure and chemical composition. *Biomaterials* **2002**, *23*, 491–501. [[CrossRef](#)]
22. Zhang, H.P.; Lu, X.; Leng, Y.; Watari, F.; Weng, J.; Feng, B.; Qu, S. Effects of aqueous environment and surface defects on Arg-Gly-Asp peptide adsorption on titanium oxide surfaces investigated by molecular dynamics simulation. *J. Biomed. Mater. Res. A* **2011**, *96*, 466–476. [[CrossRef](#)]
23. Rajh, T.; Dimitrijevic, N.M.; Bissonnette, M.; Koritarov, T.; Konda, V. Titanium dioxide in the service of the biomedical revolution. *Chem. Rev.* **2014**, *114*, 10177–10216. [[CrossRef](#)] [[PubMed](#)]
24. Liu, L.; Li, K.; Chen, X.; Liang, X.; Zheng, Y.; Li, L. Amino acid adsorption on anatase (101) surface at vacuum and aqueous solution: A density functional study. *J. Mol. Model.* **2018**, *24*, 107. [[CrossRef](#)]
25. Cucchi, A.; Molè, F.; Rinaldi, L.; Marchetti, C.; Corinaldesi, G. The Efficacy of an Anatase-Coated Collar Surface in Inhibiting the Bacterial Colonization of Oral Implants: A Pilot Prospective Study in Humans. *Int. J. Oral Maxillofac. Implants* **2018**, *33*, 395–404. [[CrossRef](#)] [[PubMed](#)]
26. Wu, C.; Chen, M.; Guo, C.; Zhao, X.; Yuan, C. Peptide-TiO₂ interaction in aqueous solution: Conformational dynamics of RGD using different water models. *J. Phys. Chem. B* **2010**, *114*, 4692–4701. [[CrossRef](#)]
27. Song, D.P.; Chen, M.J.; Liang, Y.C.; Bai, Q.S.; Chen, J.X.; Zheng, X.F.Y. Adsorption of tripeptide RGD on rutile TiO₂ nanotopography surface in aqueous solution. *Acta Biomater.* **2010**, *6*, 684–694. [[CrossRef](#)] [[PubMed](#)]
28. Wang, Q.; Wang, M.H.; Wang, K.F.; Liu, Y.; Zhang, H.P.; Lu, X.; Zhang, X.D. Computer simulation of biomolecule-biomaterial interactions at surfaces and interfaces. *Biomed. Mater.* **2015**, *10*, 032001. [[CrossRef](#)]
29. Sowmiya, M.; Senthilkumar, K. Adsorption of proline, hydroxyproline and glycine on anatase (001) surface: A first-principle study. *Theor. Chem. Acc.* **2016**, *135*, 12. [[CrossRef](#)]
30. Sowmiya, M.; Senthilkumar, K. Adsorption of RGD tripeptide on anatase (001) surface—A first principle study. *Comput. Mater. Sci.* **2015**, *104*, 124–129. [[CrossRef](#)]
31. YazdanYar, A.; Aschauer, U.; Bowen, P. Interaction of biologically relevant ions and organic molecules with titanium oxide (rutile) surfaces: A review on molecular dynamics studies. *Colloids Surf. B Biointerfaces* **2018**, *161*, 563–577. [[CrossRef](#)]
32. Luan, B.; Huynh, T.; Zhou, R. Simplified TiO₂ force fields for studies of its interaction with biomolecules. *J. Chem. Phys.* **2015**, *142*, 234102. [[CrossRef](#)]
33. Yang, W.; Xi, X.; Shen, X.; Liu, P.; Hu, Y.; Cai, K. Titania nanotubes dimensions-dependent protein adsorption and its effect on the growth of osteoblasts. *J. Biomed. Mater. Res. Part A* **2014**, *102*, 3598–3608. [[CrossRef](#)]
34. Hoyos-Nogués, M.; Falgueras-Batlle, E.; Ginebra, M.P.; Manero, J.M.; Gil, J.; Mas-Moruno, C. A Dual Molecular Biointerface Combining RGD and KRSR Sequences Improves Osteoblastic Functions by Synergizing Integrin and Cell-Membrane Proteoglycan Binding. *Int. J. Mol. Sci.* **2019**, *20*, 1429. [[CrossRef](#)] [[PubMed](#)]
35. Penna, M.J.; Mijajlovic, M.; Biggs, M.J. Molecular-level understanding of protein adsorption at the interface between water and a strongly interacting uncharged solid surface. *J. Am. Chem. Soc.* **2014**, *136*, 5323–5331. [[CrossRef](#)]
36. Polimeni, M.; Petridis, L.; Smith, J.C.; Arcangeli, C. Dynamics at a peptide–TiO₂ anatase (101) interface. *J. Phys. Chem. B* **2017**, *121*, 8869–8877. [[CrossRef](#)] [[PubMed](#)]
37. Kumar, S.; Rosenberg, J.M.; Bouzida, D.; Swendsen, R.H.; Kollman, P.A. The weighted histogram analysis method for free-energy calculations on biomolecules. I. *Method J. Comput. Chem.* **1992**, *13*, 1011–1021. [[CrossRef](#)]
38. Beutner, R.; Michael, J.; Schwenzler, B.; Scharnweber, D. Biological nano-functionalization of titanium-based biomaterial surfaces: A flexible toolbox. *J. R. Soc. Interface* **2010**, *7* (Suppl. S1), S93–S105. [[CrossRef](#)]
39. Valentin, A.H.; Weber, J. Receptor technology–cell binding to P-15: A new method of regenerating bone quickly and safely—preliminary histomorphometrical and mechanical results in sinus floor augmentations. *Keio J. Med.* **2004**, *53*, 166–171. [[CrossRef](#)] [[PubMed](#)]
40. Bell, B.F.; Schuler, M.; Tosatti, S.; Textor, M.; Schwartz, Z.; Boyan, B.D. Osteoblast response to titanium surfaces functionalized with extracellular matrix peptide biomimetics. *Clin. Oral Implants. Res.* **2011**, *22*, 865–872. [[CrossRef](#)]
41. Garcia, A.; Reyes, C. Bio-adhesive Surfaces to Promote Osteoblast Differentiation and Bone Formation. *J. Dent. Res.* **2005**, *84*, 407–413. [[CrossRef](#)]
42. Agosta, L.; Zollo, G.; Arcangeli, C.; Buonocore, F.; Gala, F.; Celino, M. Water driven adsorption of amino acids on the (101) anatase TiO₂ surface: An ab initio study. *Phys. Chem. Chem. Phys.* **2015**, *17*, 1556–1561. [[CrossRef](#)] [[PubMed](#)]
43. Schneider, J.; Ciacchi, L.C. Specific Material Recognition by Small Peptides Mediated by the Interfacial Solvent Structure. *J. Am. Chem. Soc.* **2012**, *134*, 2407–2413. [[CrossRef](#)]

44. Sumita, M.; Hu, C.; Tateyama, Y. Interface Water on TiO₂ Anatase (101) and (001) Surfaces: First-Principles Study with TiO₂ Slabs Dipped in Bulk Water. *J. Phys. Chem. C* **2010**, *114*, 18529–18537. [[CrossRef](#)]
45. Sultan, A.M.; Hughes, Z.E.; Walsh, T.R. Binding Affinities of Amino Acid Analogues at the Charged Aqueous Titania Interface: Implications for Titania-Binding Peptides. *Langmuir* **2014**, *30*, 13321–13329. [[CrossRef](#)] [[PubMed](#)]
46. Brandt, E.; Lyubartsev, A. Molecular Dynamics Simulations of Adsorption of Amino Acid Side Chain Analogues and a Titanium Binding Peptide on the TiO₂ (100) Surface. *J. Phys. Chem. C* **2015**, *119*, 18126–18139. [[CrossRef](#)]
47. Arcangeli, C.; Borriello, I.; Gianese, G.; Celino, M.; Morales, P. Organic Functionalization of Metal Oxide Surfaces: An Atomic Scale Modeling Approach. *Nanosci. Nanotechnol. Lett.* **2013**, *5*, 1147–1154. [[CrossRef](#)]
48. Lemkul, J.; Bevan, D. Assessing the Stability of Alzheimer’s Amyloid Protofibrils Using Molecular Dynamics. *J. Phys. Chem. B* **2010**, *114*, 1652–1660. [[CrossRef](#)] [[PubMed](#)]
49. Muir, J.; Costa, D.; Idriss, H. DFT computational study of the RGD peptide interaction with the rutile TiO₂ (110) surface. *Surf. Sci.* **2014**, *624*, 8–14. [[CrossRef](#)]
50. Schneider, J.; Ciacchi, L.C. A Classical Potential to Model the Adsorption of Biological Molecules on Oxidized Titanium Surfaces. *J. Chem. Theory Comput.* **2010**, *7*, 473–484. [[CrossRef](#)] [[PubMed](#)]
51. Guo, Y.-N.; Lu, X.; Zhang, H.-P.; Weng, J.; Watari, F.; Leng, Y. DFT Study of the Adsorption of Aspartic Acid on Pure, N-Doped, and Ca-Doped Rutile (110) Surfaces. *J. Phys. Chem. C* **2011**, *115*, 18572–18581. [[CrossRef](#)]
52. Barczyk, M.; Carracedo, S.; Gullberg, D. Integrins. *Cell Tissue Res.* **2010**, *339*, 269–280. [[CrossRef](#)]
53. Bekker, H.; Berendsen, H.J.C.; Dijkstra, E.J.; Achterop, S.; van Druenen, R.; van der Spoel, D.; Sijbers, A.; Keegstra, H.; Reitsma, B.; Renardus, M.K.R. *Gromacs: A Parallel Computer for Molecular Dynamics Simulations*; Physics Computing 92; de Groot, R.A., Nadrchal, J., Eds.; World Scientific: Singapore, 1993.
54. Berendsen, H.J.C.; Van Der Spoel, D.; Van Druenen, R. GROMACS: A message-passing parallel molecular dynamics implementation. *Comput. Phys. Commun.* **1995**, *91*, 43–56. [[CrossRef](#)]
55. Lindahl, E.; Hess, B.; van der Spoel, D. GROMACS 3.0: A package for molecular simulation and trajectory analysis. *J. Mol. Mod.* **2001**, *7*, 306–317. [[CrossRef](#)]
56. Van Der Spoel, D.; Lindahl, E.; Hess, B.; Groenhof, G.; Mark, A.E.; Berendsen, H.J.C. GROMACS: Fast, flexible, and free. *J. Comput. Chem.* **2005**, *26*, 1701–1718. [[CrossRef](#)]
57. Hess, B.; Kutzner, C.; Van Der Spoel, D.; Lindahl, E. GROMACS 4: Algorithms for Highly Efficient, Load-Balanced, and Scalable Molecular Simulation. *J. Chem. Theory Comput.* **2008**, *4*, 435–447. [[CrossRef](#)] [[PubMed](#)]
58. Pronk, S.; Páll, S.; Schulz, R.; Larsson, P.; Bjelkmar, P.; Apostolov, R.; Shirts, M.R.; Smith, J.C.; Kasson, P.M.; Van Der Spoel, D.; et al. GROMACS 4.5: A high-throughput and highly parallel open source molecular simulation toolkit. *Bioinformatics* **2013**, *29*, 845–854. [[CrossRef](#)]
59. Páll, S.; Abraham, M.J.; Kutzner, C.; Hess, B.; Lindahl, E. Tackling exascale software challenges in molecular dynamics simulations with GROMACS. In *Solving Software Challenges for Exascale*; Markidis, S., Laure, E., Eds.; Springer International Publishing: London, UK; Cham, Switzerland, 2015; Volume 8759, pp. 3–27.
60. Abraham, M.J.; Murtola, T.; Schulz, R.; Páll, S.; Smith, J.C.; Hess, B.; Lindahl, E. GROMACS: High performance molecular simulations through multi-level parallelism from laptops to supercomputers. *SoftwareX* **2015**, *1–2*, 19–25. [[CrossRef](#)]
61. MacKerell, A.D., Jr.; Bashford, D.; Bellott, M.L.D.R.; Dunbrack, R.L., Jr.; Evanseck, J.D.; Field, M.J.; Fischer, S.; Gao, J.; Guo, H.; Ha, S.; et al. All-atom empirical potential for molecular modeling and dynamics studies of proteins. *J. Phys. Chem. B* **1998**, *102*, 3586–3616. [[CrossRef](#)]
62. Huang, J.; Rauscher, S.; Nawrocki, G.; Ran, T.; Feig, G.N.M.; De Groot, B.L.; Grubmüller, S., Jr. CHARMM36m: An improved force field for folded and intrinsically disordered proteins. *Nat. Methods* **2017**, *14*, 71–73. [[CrossRef](#)] [[PubMed](#)]
63. Howard, C.J.; Sabine, T.M.; Dickson, F. Structural and thermal parameters for rutile and anatase. *Acta Crystallogr. Sect. B Struct. Sci.* **1991**, *47*, 462–468. [[CrossRef](#)]
64. Allouche, A.-R. Gabedit-A graphical user interface for computational chemistry softwares. *J. Comput. Chem.* **2011**, *32*, 174–182. [[CrossRef](#)] [[PubMed](#)]
65. Jorgensen, W.L.; Chandrasekhar, J.; Madura, J.D.; Impey, R.W.; Klein, M.L. Comparison of simple potential functions for simulating liquid water. *J. Chem. Phys.* **1983**, *79*, 926–935. [[CrossRef](#)]
66. Loncharich, R.J.; Brooks, B.R.; Pastor, R.W. Langevin dynamics of peptides: The frictional dependence of isomerization rates of *N*-acetylalanine-*N'*-methylamide. *Biopolymer* **1992**, *32*, 523–535. [[CrossRef](#)] [[PubMed](#)]
67. Hub, J.S.; Awasthi, N. Probing a Continuous Polar Defect: A Reaction Coordinate for Pore Formation in Lipid Membranes. *J. Chem. Theory Comput.* **2017**, *13*, 2352–2366. [[CrossRef](#)] [[PubMed](#)]